Design of Small Intramolecular Singlet Fission Chromophore: An Azaborine Candidate and General Small Size Effects

Tao Zeng*,† and Prateek Goel‡

†*Department of Chemistry, Carleton University, Ottawa, Ontario, K1S5B6, Canada*

‡*Department of Chemistry, University of Waterloo, Waterloo, Ontario, N2L3G1, Canada*

E-mail: toby.zeng@carleton.ca

Abstract

We report the first attempt to design small *intra*molecular singlet fission chromophores, with the aid of quantum chemistry and explicitly simulating the time evolution of state populations using quantum dynamics method. We start with three previously proposed azaborine-substituted *inter*molecular singlet fission chromophores. Through analyzing their frontier orbital amplitudes, we select a BN-substituted azulene as the building block. Covalently connecting two such monomers and tuning their relative configuration, we examine three dimers. One dimer is found to be an eminent candidate: the triplet-pair state is quickly formed within 1 ps; the two triplets are ready to be disentangled. We elucidate the general small size effects in intramolecular singlet fission, and focus on specific aspects which should be taken care of when manipulating the fission rate through steric hindrance.

Graphical TOC Entry

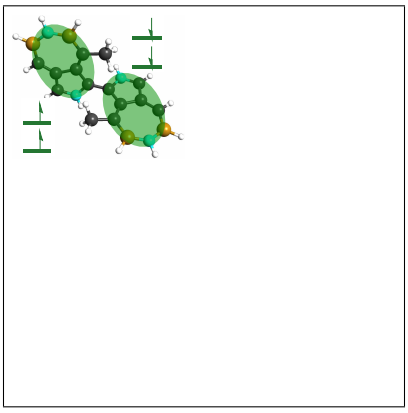

Keywords

Singlet Fission; Small Chromophore; Azaborine Chemistry; Non-Adiabatic Dynamics; Multireference Perturbation Theory; Multi-Configurational Time-Dependent Hartree

Singlet fission (SF) converts one singlet exciton to two triplet excitons.[1,2] The implied number doubling and life lengthening of excitons make SF a promising avenue to surpass the ∼32% Shockley-Queisser[3] limit for energy conversion efficiency of single junction solar cells, and realize the third generation of solar cells.[1,2,4–6] The SF process is schematically demonstrated in Figure 1 using a 2 chromophores 4 orbitals 4 electrons picture. The single-*e*xcitonic *eg* and *ge* states that contain only one singlet excited chromophore first convert to the multi-excitonic *tt* state, with two *t*riplet excitons on the two chromophores and forming an overall singlet state. This spin-conserved step can go through the direct and the charge-transfer (CT) mediated pathways. The latter is usually more pronounced and involves the *ca* and *ac* states,[7,8] for which *c* and *a* stand for *c*ation and *a*nion. The two triplet excitons are then disentangled by spin-dependent operators and thermalization to have random orientations of their spins, resulting in the $t + t$ state.[9] See Section S1 in the Supporting Information (SI) for more general discussion of SF.

So far, most of the effort has been dedicated to intermolecular singlet fission (xSF,"x" for external) studies, that the SF occurs among more than one chromophore molecule. xSF usually occurs in solids of chromophores, and SF's sensitivity to the intermolecular configuration of its participants[10–12] is translated to a dependence on the morphology of the solid materials,[13–15] which is "onerous to control experimentally."[16] Considering the power of synthetic chemists in controlling molecular configuration, an alternative route of intramolecular singlet fission (iSF) was recently proposed. The central idea is to attain SF-favoured inter-chromophore configuration through the more controllable covalent bonding and intramolecular steric effects, so that the difficulty of controlling crystal packing and morphology can be circumvented.[17] iSF occurs within one photo-excited molecule, with the two resultant triplet excitons located on different moieties within the molecule.[18–22] In 2015, several groups made significant breakthroughs in this direction and synthesized materials that feature $> 150\%$ iSF yield,[23–28] which is the number of triplet excitons generated per absorbed photon.

A major obstacle in the field of SF is the paucity of SF-capable materials,[16,17] and a

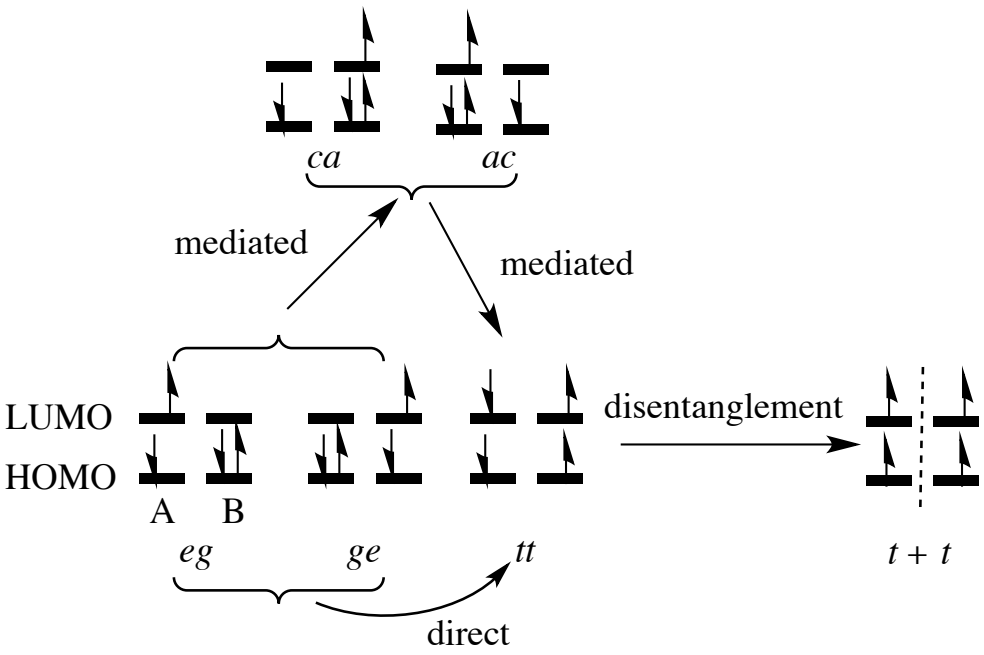

Figure 1: Electronic configuration prototypes involved in singlet fission and the discussion in this paper. "A" and "B" denote the two chromophores (or chromophore units in *i*SF) that undergo SF. Horizontal bars represent frontier orbital levels in the two monomers. Vertical arrows denote electronic spin-up and -down. The arrows with "direct" and "mediated" represent the two pathways in the spin-conserved step. The dashed line in the $t + t$ state means that the two triplet excitons have been disentangled.

number of new SF chromophore designs have been proposed in the recent past.[29–32] Chromophores of small size are especially interesting because: their theoretical studies are less resource-demanding, and they can serve as models to reveal fundamental SF mechanisms; small systems are usually, but definitely not always, easier to synthesize and process; in practice, small chromophores implies high exciton density by weight and volume, facilitating the development of mini photovoltaic devices. Michl *et al.* pioneered this direction of research and proposed heterocyclic diradicaloid *x*SF chromophores with only about 10 non-hydrogen atoms.[29,30] Other *x*SF designs based on azaborine-substitution[31] and monosilicon-substitution[32] have also been proposed.

To our knowledge, no attempt has been made to design small *i*SF chromophores. This fact motivates us to carry out the present theoretical research. Aside from designing the specific chromophores, we address the following questions: (1) where are the appropriate

sites to covalently connect two identical small SF chromophore units? (2) how to tune the structure so that the triplet-pair can be appropriately coupled with other electronic configurations, facilitating the separation of the pair? (3) what are the unique characters of small *i*SF chromophores compared to their large counterparts. Our study is based on the recently proposed azaborine-substituted molecules.[31] Azaborine chemistry is a rapidly advancing field,[33–38] and the potential application of azaborine-substituted molecules in singlet fission is starting to be realized.[39] We hope that this study will further crosslink the two vibrant fields and lead to fruitful results in the future.

Details of computational methods are given in Section S2 in SI. In brief, structural optimization is carried out with the M06-2X density functional.[40] The General Multi-Configurational Quasi-Degenerate Perturbation Theory (GMC-QDPT)[41–43] is used to calculate energies and wave functions of low-lying electronic states. The states are diabatized[44] to generate diabatic states (diabats) that are dominated by and named after the configurations shown in Figure 1. All electronic structure calculations are performed using the cc-pVDZ basis set[45] and the GAMESS-US program package.[46,47] The Multi-Configurational Time-Dependent Hartree (MCTDH) method[48,49] is used to simulate the *i*SF dynamics of the chromophore designs, focusing on how fast and how much the *tt* configuration is populated.

Which chromophore(s) and where to connect them? — We aim at covalently connecting two identical small constituent chromophores (homodimers), so that symmetry can be exploited to facilitate calculations. Also, homodimers of small chromophores already tend to have low energy CT states that bind the two generated triplets (see below). Connecting different chromophores (heterodimers) is likely to further lower the CT energy[21] and bind the triplets more strongly, impeding their disentanglement and separation. To minimize the *i*SF chromophore, we would like to connect the two constituents directly without any spacer. The three azaborine-substituted chromophores proposed before are shown in Figure 2 along with their highest occupied and lowest unoccupied molecular orbitals (HOMO and LUMO). The B and N atoms serve as electron-acceptor and -donor that captodatively[50,51] strengthen

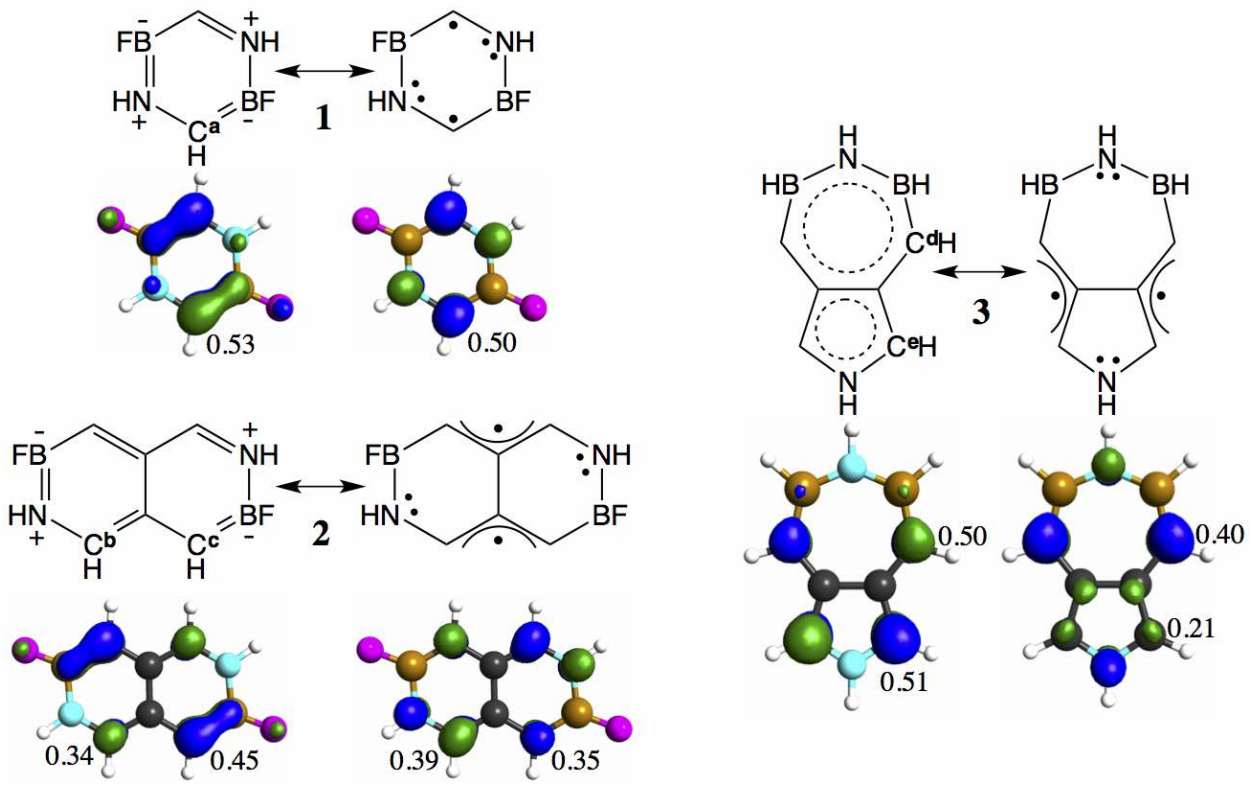

Figure 2: The three azaborine small SF chromophores proposed in Ref. 31. In addition to the conventional Kekulé or aromatic structure, another resonance structure is also given for each chromophore to highlight its diradical character. Under each chromophore are isosurfaces of its HOMO (left) and LUMO (right). The H, B, C, N, and F atoms are represented by white, brown, gray, cyan, and purple spheres. Blue and green indicate orbital phases. Symmetrically unique C atoms in each structure are labeled by superscripts. Numbers in the orbital pictures are the approximate amplitudes (in atomic unit, sign ignored) of the orbitals on those C sites.

the diradical character of the molecules to make them feature exoergic SF. To maintain this character for the monomers, we only consider C atoms as the connecting sites.

The effective coupling matrix element between eg/ge and tt determines the CT-mediated SF rate,[1,2,8] and it is proportional to

$$\frac{t_{HL}t_{LL} - t_{LH}t_{HH}}{\Delta E_{CT}}. \tag{1}$$

Here t_{HL} stands for the $t$ransfer integral between the HOMO of one constituent chromophore and the LUMO of the other, i.e., the Fock matrix element of the two orbitals. t_{LH}, t_{LL}, and

t_{HH} have similar meanings. ΔE_{CT} stands for the energy difference between the mediating CT state and the single-excitonic state. If two constituents are symmetrically connected, $t_{HL} = t_{LH}$. $t_{LL} \neq t_{HH}$ is thus necessary to open the CT-mediated pathway.[21,52,53] Figure 2 shows that the C^e site of **3** features the largest difference in HOMO and LUMO amplitudes, which suggests the largest magnitude of $t_{LL} - t_{HH}$. Therefore, C^e is the most ideal connecting site, and **3** the best candidate to construct a covalent dimer for *i*SF. In below, we concentrate on the so-connected **4** and its derivatives in searching for good *i*SF chromophores.

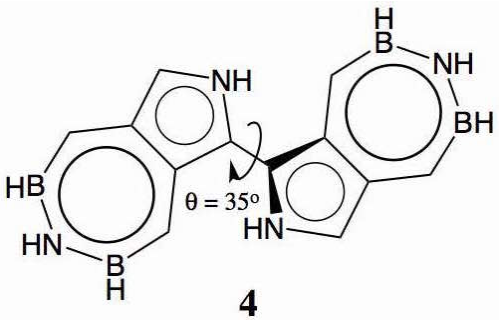

4

4 *itself* — The coordinates of **4** and the other dimers are given in Section S15 in SI. Overall, each constituent BN-substituted azulene retains its monomer structure. It is of C_2 symmetry and the dihedral angle between the two BN-azulenes about the connecting C-C bond (θ) is 35°. $\theta = 0°$ corresponds to the C_{2h} *trans*-structure. The HOMO−1 and HOMO of **4** are the bonding and antibonding combinations of the two **3** units' HOMOs (Figure S2 in SI); the LUMO and LUMO+1 are the analogues of the monomers' LUMOs. The interconnecting C-C bond is 1.44 Å long, close to the typical 1.47 Å C-C single bond between two sp^2 C atoms.[54]

The diabatic Hamiltonian matrix of **4** at its optimized structure is

$$\begin{array}{c} \\ tt \\ xta \\ xtb \\ cta \\ ctb \end{array} \begin{array}{c} \begin{array}{ccccc} tt & xta & xtb & cta & ctb \end{array} \\ \begin{pmatrix} 1.51 & -0.08 & 0.00 & 0.24 & 0.00 \\ -0.08 & 2.00 & 0.00 & 0.57 & 0.00 \\ 0.00 & 0.00 & 2.08 & 0.00 & -0.58 \\ 0.24 & 0.57 & 0.00 & 2.34 & 0.00 \\ 0.00 & 0.00 & -0.58 & 0.00 & 2.52 \end{pmatrix} \end{array} . \tag{2}$$

eV is used as the energy unit and the diagonal energies are relative to the ground state energy. The same convention is followed throughout this paper. Here, a symmetry-adapted diabatic representation has been used: *tt* is symmetry-adapted already and transforms following the *A* irreducible representation (irrep) of the C_2 point group; *xta* and *xtb* are the linear combinations of *eg* and *ge* that transform following the *A* and *B* irreps; *cta* and *ctb* are the analogues of *ca* and *ac*. In this concise representation, the target state *tt* is only coupled to *xta* and *cta*, while in the representation using the local states in Figure 1, *tt* is coupled to all the other four (Eq. S3 in SI).

Scheme 1

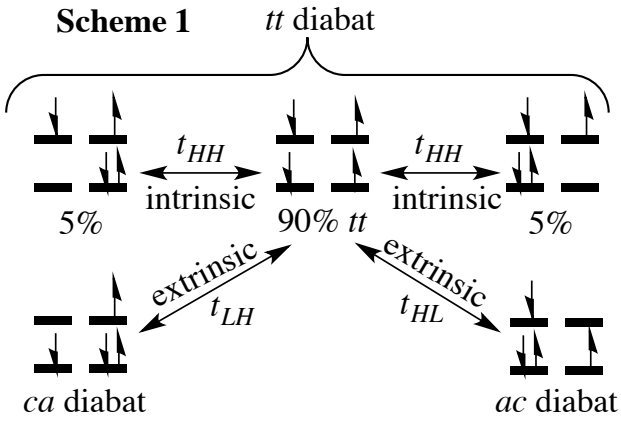

Evidently, *tt* is the lowest in energy amongst the five diabats, suggesting an exoergic *i*SF. It however seems too exoergic: *tt* is ∼0.5 eV lower than *xta* and *xtb*, while for the **3** monomer, $E(S_1) - 2E(T_1) = 0.09$ eV (Section S3 in SI; S_1 and T_1, the lowest singlet and

triplet excited states). This significant energy lowering is attributed to the 9 : 1 mixture of the *tt* and two CT configurations other than *ca* and *ac* within the *tt* diabat, as shown in Scheme 1. The mixing stems from the −0.88 eV large t_{HH} (Eq. S1 in SI), which results from **4**'s quasi-planar structure and **3**'s large HOMO amplitude at the interconnecting site. This coupling occurs within one diabat and we call it "intrinsic coupling", to differentiate it from the "extrinsic couplings" between diabats. The two types of coupling in **4** are illustrated in Scheme 1 and more discussion is given in Section S6 in SI. The large HOMO amplitude arises from the concentration of the orbitals in the small monomers. In comparison, we evaluate the HOMO and LUMO amplitudes of pentacene at the interconnecting site in bis-pentacene in Ref. 26 to be only ∼0.13, and the stabilization of the multi-excitonic state is expected to be smaller.

Along with the large intrinsic coupling in *tt* are the substantial extrinsic couplings, 0.24 eV between *tt* and *cta*, 0.57 eV between the *xta* and *cta*, and −0.58 eV between *xtb* and *ctb*. All these couplings are approximately proportional to the cross-monomer transfer integrals t_{HH}, t_{HL}, and t_{LL} (see Eqs. S1 and S2 in SI for their values).[1,2] Again, the larger frontier orbital amplitudes at the interconnecting sites, due to the small size of **3**, are responsible for these large couplings. Even the usually negligible *tt*-*xta* coupling that involves two-electron integral of cross-monomer electron density[1,2] is as large in magnitude as −0.08 eV.

The small size of **4** favours low energy CT configurations. The positive and negative charge densities are concentrated in the small **3** moieties and the geometrical centers between the two moieties are not far apart. Substantial Coulombic stabilization of the CT diabats is expected. In fact, *cta* is only 0.26 eV higher than *xtb* and it can actively mediate the conversion from the two *xt* diabats to *tt*. In comparison, the CT states in the TIPS-pentacene dimer investigated by Sanders *et al.*[26] have the opposite charges dispersed over the respective large pentacene derivatives. The short-edge connection also leads to a far 14 Å distance between the geometrical centers of the charges. Correspondingly, the CT states are ∼1 eV above the single-excitonic states and cannot mediate SF. In general, the CT

states should be more influential in *i*SF of small chromophores due to their low energies and the large inter-monomer transfer integrals that couple them to the single and multi-excitonic states. The influence is double-sided: if the CT states are too strongly coupled with tt, they hinder the disentanglement of the two triplets. Indeed, the coupling between tt and any CT configurations (e.g., Configurations 7 to 14 in Figure S3 in SI), intrinsic or extrinsic, can be understood as binding of the triplet pair.[9]

The initial electronic state of the *i*SF dynamics simulation should be the lowest "bright" adiabatic state that has a large transition dipole moment connected to the ground state. The S_0-to-S_1 (S_0 stands for ground state) transition dipole of **3** is along the ring-shared C-C bond. Since the two such C-C bonds in **4** are largely perpendicular to the C_2 axis, the addition of the two **3** moieties' transition dipoles determines the lowest bright state to be a B state. Such a bright state is the S_2 state of **4**, and its excitation energy and oscillator strengths are evaluated to be 1.67 eV and 0.43. In comparison, the oscillator strengths of the surrounding A states are all < 0.007.

To have an appropriate initial electronic state for the MCTDH simulation, we choose another diabatic representation, in which the electronic Hamiltonian matrix reads

$$
\begin{array}{c} \\ tt \\ xta' \\ xtb' \\ cta' \\ ctb' \end{array}
\begin{array}{c}
\begin{array}{ccccc} tt & xta' & xtb' & cta' & ctb' \end{array} \\
\left(\begin{array}{ccccc}
1.51 & -0.21 & 0.00 & 0.15 & 0.00 \\
-0.21 & 1.57 & 0.00 & 0.00 & 0.00 \\
0.00 & 0.00 & 1.68 & 0.00 & 0.00 \\
0.15 & 0.00 & 0.00 & 2.78 & 0.00 \\
0.00 & 0.00 & 0.00 & 0.00 & 2.92
\end{array}\right)
\end{array}
. \tag{3}
$$

xta' and cta' are states that diagonalize the xta and cta block in Eq. 2; The prime of xta' indicates that it contains more xta component than cta, while cta' is the other way around. xtb' and ctb' are defined similarly. This semi-diagonal representation gives us xtb' as the lowest bright **adiabatic** state in the vertical excitation and the optimal choice as

the initial electronic state for the dynamics simulation. It also brings xta' and xtb' closer in energy to tt, while cta' and ctb' higher up. The highest ctb' is weakly coupled to the other states only through vibronic coupling, and is discarded in the dynamics simulation to reduce computational effort. The exclusion of ctb' does not suppress the CT-mediating SF pathway, as xtb' contains ctb's contribution. We keep cta' in the simulation, and the wave packet on this high-lying transiently populated diabat can be described using a small number of single particle functions (SPFs) in MCTDH simulation.[55] We emphasize that those semi-diagonal diabats only diagonalize the respective sub-blocks at the S_0 structure. As the structure is distorted, the sub-blocks become nonzero. The summary and comparison of the different diabatic representations are given in Section S7 in SI. tt remains the same in all representations.

Our vibronic coupling Hamiltonian to describe iSF dynamics and the vibrational modes selection are detailed in Section S8 in SI. In brief, it contains linear vibronic coupling; dimer normal modes that reflect the structural distortion in the monomer's S_0-to-S_1 and S_0-to-T_1 excitations are included, and also the inter-monomer torsional mode that modulates the transfer integrals t_{HH}, t_{HL}, and t_{LL}. The iSF dynamics starts with a B state (xtb') and the objective state is an A state (tt). The b-modes are the coupling modes for the transition from the B state to the A manifold, while the a-modes are tuning modes. Taking the S_0's ground vibrational state as the initial wave packet on xtb', we run a 2 ps MCTDH simulation. The population evolution of the four diabats is shown in Figure 3. The eventual tt population is relatively low. The significant 0.75:0.20 eventual tt-xta' mixing can be traced back to their -0.21 eV strong coupling and 0.06 eV small energy distance. Considering only these electronic matrix elements leads to a $60:40$ tt-xta' mixing. The two states are differently coupled to the vibrational modes, giving 0.44 and 0.16 eV reorganization energies of tt and xta'. These different couplings reduce the mixing but not completely. The consideration of the intrinsic coupling in the tt diabat scales the genuine tt population down by 0.9 to 0.68, which is represented by the "X" marker in Figure 3. These mixings, intrinsic and

extrinsic, hinder the disentanglement of the two triplet excitons. In this sense, **4** is very similar to tetracyanoquinodimethane bithiophene, which features a fast non-radiative decay from the lowest bright state to a "dark state" that contains a large portion of multi-exciton character,[56] but also a substantial portion of other configurations.[57]

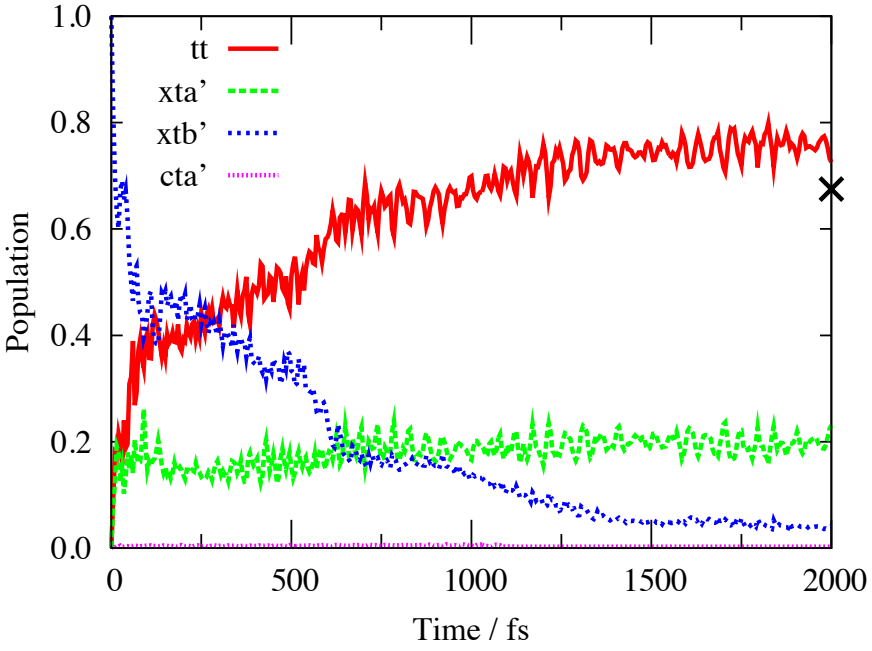

Figure 3: The MCTDH evolution of the diabats' populations of **4**. The "X" marker at 2000 fs indicates the scaled eventual *tt* population after considering the intrinsic coupling in the *tt* diabat.

Now let us review the problems of **4**. The 35° dihedral angle around the interconnecting bond leaves large overlap between the frontier orbitals of the two **3** units. They are responsible for the large intrinsic coupling in *tt* and its too low energy; also the substantial mixing between *tt* and xta'. Both effects reduce the eventual population of the *tt* configuration and impede disentanglement of the two triplet excitons. To derive a good *i*SF chromophore from **4**, we need to reduce the overlaps. A natural way is to enlarge the dihedral angle θ and make the two **3** units more orthogonal to each other.

Methylation on N — Our first attempt to "orthogonalize" the two **3** units is to methylate the 5-membered ring N (Structure **5**, Figure 4(a)). The steric repulsion between the methyl group on one unit and the 7-membered ring on the other increases the dihedral angle to 64°.

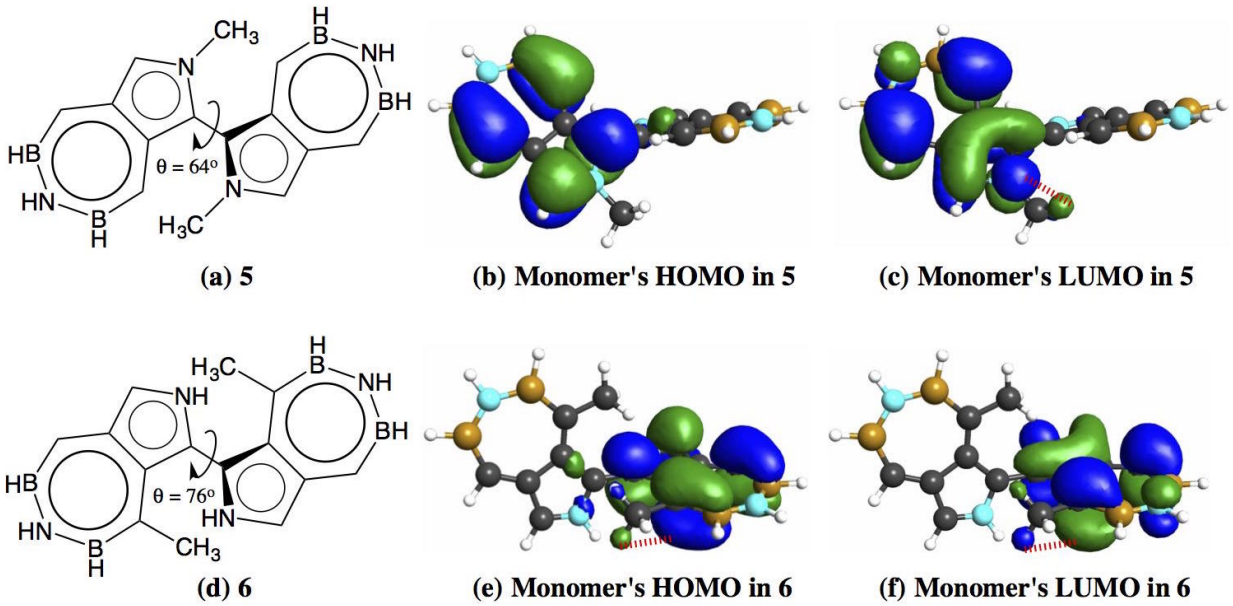

Figure 4: Sketch of Structures **5** and **6** and their monomers' frontier orbitals. Wedged bonds are used to show the non-planarity of the two methylated-**3** units. Each **3** unit remains planar, except the three H atoms on the methyl. The red hashed lines indicate the antibonding interaction between the methyl and the HOMO and LUMO of **3**. The H, B, C, and N atoms are represented by white, brown, gray, and cyan spheres. Blue and green indicate orbital phases.

The electronic Hamiltonian matrices in both the symmetry-adapted and the semi-diagonal diabatic representations at the ground state structure are given in Eqs. S9 and S10.

As expected, all off-diagonal elements in the symmetry-adapted representation are smaller than the counterparts of **4** (Eq. S9 vs. Eq. 2, also compare Eqs. S1 and S12 in SI for the reduction of the inter-monomer transfer integrals). The intrinsic coupling in tt is also reduced; the diabat contains 97% tt configuration. However, the tt energy now seems too high. In the semi-diagonal representation (Eq. S10), tt is higher in energy than both xta' and xtb' by ∼0.07 eV. The iSF of **5** is still exoergic, since tt's reorganization energy is 0.44 eV, much larger than the 0.16 and 0.19 eV of the xta' and xtb' counterparts.

The evolution of state populations of **5** is shown in Figure 5. Regardless of the θ value, the two substituent transition dipoles of the monomers are largely perpendicular to the C_2 axis. Therefore, xtb' is still the lowest bright and initial state for the MCTDH simulation. Despite the 30° larger θ, this methylation moderately increases the eventual tt population

from 0.68 to 0.76, which has been scaled by the 97% percentage of tt configuration in the tt diabat. The extrinsic couplings are certainly not small enough and a larger θ is needed. The unanticipated high tt energy is another reason for this small population increase. tt is 0.06 eV higher than xta' at the Franck-Condon region and their -0.10 eV coupling give them a 44:56 mixing. The two diabats relax in the same direction along the modes that feature large diagonal vibronic coupling constants. For example, the 1556 and 1607 cm^{-1} a-modes give the largest vibonic coupling constants, ~ -0.2 and ~ -0.1 eV, for the tt and xta' diabats (Section S14.B in SI); they are both negative. The same direction relaxation inhibits their decoupling.

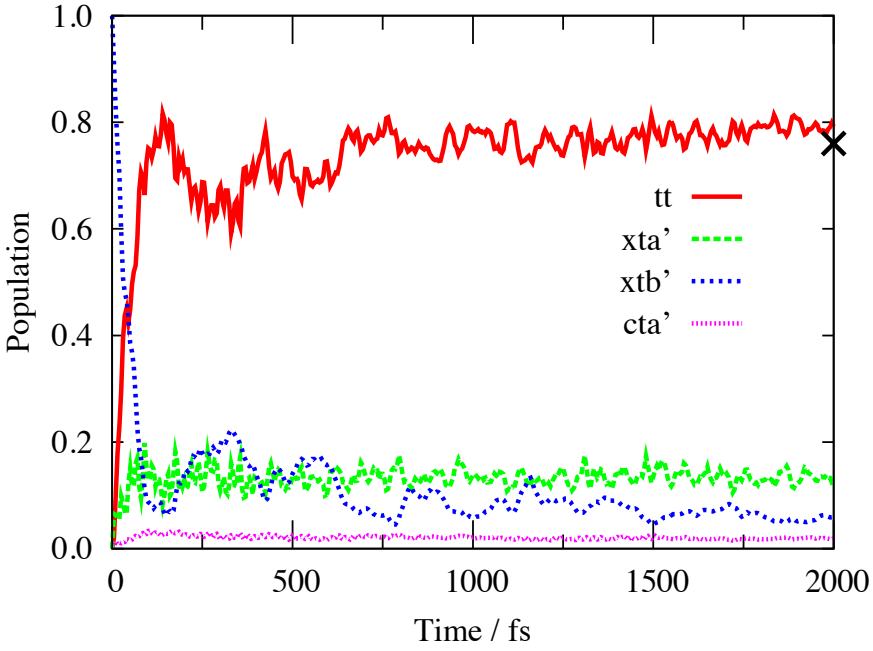

Figure 5: The MCTDH evolution of the diabats' populations of **5**. The "X" markers at 2000 fs indicate the scaled eventual tt populations after considering the intrinsic coupling in the tt diabats.

If we replace the two methyls in **5** by H (**5H**) and keep all the other structural parameters identical to **5**, the tt energy is lowered from 1.84 to 1.72 eV, and the eventual tt population is raised to 0.81. The methylation has certainly done more than just enlarging θ. The effects of the methylation on the diabatic energies are analyzed based on an orbital interaction picture in Section S9 in SI. In short, the methyl induces an antibonding interaction with

the **3** unit's LUMO, but not with the HOMO (see Figure 4(b) and (c)). The consequent unbalanced energy raising of the monomer's frontier orbitals results in the high *tt* energy. The methyls also increase the inter-monomer Coulombic attraction and lower the *cta* and *ctb* energies, due to the closer spatial contact of the HOMO and LUMO on the two monomers Section S9. Overall, the proximity in energy of *tt*, *xta*, and *cta* counteracts the reduction of their extrinsic couplings, making it difficult to separate *tt* from the others.

Even the neutral and mild substituent, methyl, delivers side effects in addition to steric hindrance. The small chromophore size again plays a role. If the monomer frontier orbitals were delocalized over a larger unit and their amplitudes reachable by the methyls, or in general, bulky groups, are correspondingly reduced, those side effects on electronic structure would be mitigated, and the methyls would only induce steric hindrance to give a desirable structure. This nontrivial difference between small and large *i*SF chromophores shall be kept in mind for future works in this direction.

Methylation on C — Guided by the failure of **5**, we try another structure with the two methyls on the 7-membered rings as shown in Structure **6** (Figure 4(d)). The motivation is that **3**'s HOMO and LUMO have similar 0.50 and 0.40 amplitudes (Figure 2) on the methylated C site, so that both experience antibonding interaction from the methyl CH bonds (Figure 4(e) and (f). A detailed orbital interaction analysis is given in Section S10 in SI.). The undesired high *tt* energy may hence be avoided. The steric repulsion between the methyls and the 5-membered rings on the opposite units increases the dihedral angle to 76°. The longer CC bond between the methyl and C^d (Figure 2) than the NC bond in **5**, 1.51 vs. 1.45 Å, makes the methyls more protruding, resulting in more steric hindrance; the two units are 12° more orthogonal to each other than in **5**.

The diabatic electronic Hamiltonian matrices in the symmetry-adapted and the semi-diagonal representations at **6**'s S_0 structure are given in Eqs. S15 and S16 in the SI. Consistent with the more orthogonal structure, all couplings are further reduced compared to **5** (Eq. S15 vs. Eq. S9, also compare Eqs. S12 and S18 in SI for the reduction of the inter-monomer

transfer integrals). The *tt* energy is 1.82 eV, very close to the 1.85 eV of Structure **6H**, which has **6**'s structure but with the methyls replaced by H atoms: the extra increase of the *tt* energy not due to the dihedral angle change is indeed avoided. There is no intrinsic coupling in the *tt* diabat; it contains 100% *tt* configuration after rounding.

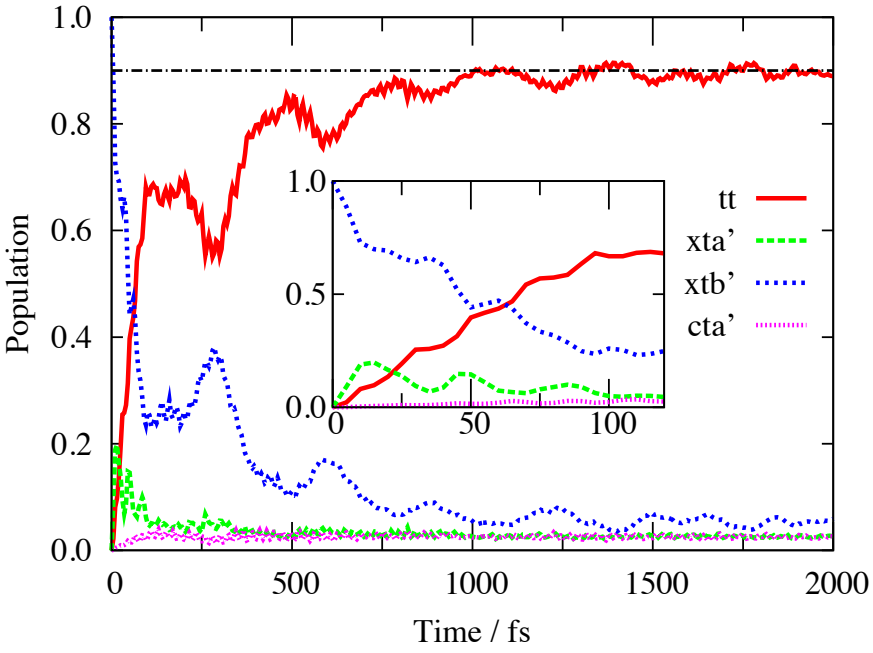

Figure 6: The MCTDH evolution of the diabats' populations of **6**. The dot-dashed horizontal line indicates the 0.9 plateau of the *tt* population.

The evolution of state populations of **6** is shown in Figure 6. The 0.9 eventual *tt* population is a significant improvement compared to **4** and **5**. The *tt* configuration is largely separated from the others in terms of both intrinsic and extrinsic coupling, and is a prominent precursor for spin disentanglement.

The *tt* population plateaus at around 1 ps, indicating an efficient *i*SF process. It quickly rises to 0.7 within 100 fs. Photoinduced absorption with the *tt* character should be observable after this time elapse. The role of xta' in this ultrafast rise-up is different from at the later time. Figure 6 and its inset show that in the first 100 fs, the xta' population oscillates with a period of ∼35 fs and with amplitude > 0.1. This is a Rabi oscillation between xta' and xtb' induced by their pseudo-degeneracy and the two 888 and 906 cm^{-1} *b*-modes, whose

vibrational periods are 37 and 36 fs (Section S11 in SI). In the later time, the oscillation is no longer seen. xta' is then like cta', a virtual state mediating the transition between xtb' and tt. xta' is more strongly coupled to xtb' through vibronic interaction due to their smaller energy distance, while cta' is more strongly coupled to tt through the electronic Hamiltonian (Eq. S16). Both channels contribute to SF.

To assure that including the only four diabats in the MCTDH simulation is adequate, we extend the vibronic model to include eight diabats and the same sets of modes, which are described by smaller numbers of SPFs. The results are presented in Section S12 in the SI. The population evolution profile resembles Figure 6; all diabats other than the four are not populated. The negligible occupation of the diabat that closely resembles the ground state indicates that the non-radiative decay channel is not competitive with the iSF in **6**.

The high eventual tt population suggests that the spin-conserved step leaves us an adiabatic state mainly derived from tt, which is the S_1 state of **6**. The C_2 symmetry of **6** determines that the spin disentanglement occurs through spin-flipping between S_1 and Q_1 (the lowest quintet adiabatic state), and the spin-flipping rate depends on the S_1-Q_1 energy gap.[1] The minimum-to-minimum energy gap between the two states is evaluated to be 0.03 eV (Section S13 in SI). This is well within the energy released in the spin-conserved step, which is approximately the sum of the 0.09 eV xtb'-tt energy gap at the S_0 structure and tt's 0.52 eV reorganization energy. Therefore, the spin disentanglement is expected to be an efficient process that occurs during the dissipation of the vibrational energy on S_1. The relatively small S_1-Q_1 gap is attributed to the two methyls that prevent further lowering of the S_1 energy (see more details in Section S13 in SI).

At **6**'s S_0 structure, the adiabatic state derived from xtb' is the S_2 state. Its vertical excitation energy is 1.91 eV, with a large 0.50 oscillator strength. The photon flux of the terrestrial solar spectrum at this red frequency is fairly high, $\sim$25 mA/m^{2}eV.[58] These features support **6** to be a good iSF chromophore.

Conclusions — We employ quantum chemistry calculation and molecular quantum dy-

namics simulation to design small azaborine-substituted singlet fission chromophores. The consideration of a viable charge-transfer SF pathway and the analysis of the HOMO and LUMO amplitudes on the possible connecting sites makes us choose an azaborine-substituted azulene (**3**) as the monomer chromophore to be covalently connected. We construct three dimers based on **3**, and one (**6**) is found to be an eminent candidate for further pursuit: it features efficient (in 1 ps) and complete (90%) single- to multi-excitonic state transition; its singlet and quintet multi-excitonic states are close in energy, so that the vibrational energy released in the *i*SF is enough to facilitate the spin disentanglement; it has intense absorption in the appropriate region of the solar spectrum.

We hope that this study will motivate azaborine chemists to synthesize the proposed molecule and enrich the highly limited collection of intramolecular singlet fission chromophores. Before this goal is achieved, this work will still be beneficial for other *i*SF studies, as what we have learned about the small size effects on *i*SF dynamics from the failures of **4** and **5** is generalizable knowledge: (1) couplings between the multi-excitonic configurations and the others are generally strong, hindering the triplet-triplet separation; (2) charge-transfer states are generally low-lying in energy. They may bind the two triplets too strongly. In the way to attain **6**, we have shown that the negative impacts in these two points can be mitigated through modulating molecular structure; (3) in modulating chromophore structure, substituents can deliver more than steric hindrance. Careful selection of substitution sites is needed to exert the desired steric hindrance and avoid the undesired modification of the energy levels. All these features of small *i*SF chromophores can be traced to their concentrated frontier orbitals confined in a compact region.

ASSOCIATED CONTENT

Supporting information The supporting information is available free of charge *via* the Internet at http://pubs.acs.org.

More introduction to singlet fission; computational methods; selection of active space; **4**'s frontier orbitals and local diabatic representation of electronic Hamiltonian matrix; details of diabatization scheme; intrinsic vs. extrinsic couplings; summary and comparison of the different diabatic representations; vibronic model and selection of vibrational modes in MCTDH simulation; how the methyls affect the *tt* energies of **5** and **6**; diabatic population transfer in the first 100 fs of *i*SF in **6**; MCTDH simulation with eight diabats for **6**; S_1 and Q_1 energies of **6**; vibronic coupling constants in the MCTDH simulations; coordinates of **4**, **5**, and **6**.

NOTE

The authors declare no competing financial interest.

ACKNOWLEDGEMENTS

T.Z. is grateful for the support of a start-up grant from Carleton University (186853). We thank Shaorong Li (University of Minnesota) and West Aaron (Iowa State University) for discussions about diabatization. We thank Marcel Nooijen (University of Waterloo) for insightful comments on the paper. We thank Mike Schmidt and Mark Gordon (Iowa State University) for their continuous support of the GAMESS-US program package. T.Z. is especially grateful to Mike for his help in programming in GAMESS. We also thank Hans-Dieter Meyer (Universität Heidelberg) for his generosity of providing the MCTDH package to us. We thank Compute Canada and Calcul Québec for computational resources, and their staffs for intellectual support.

References

(1) Smith, M. B.; Michl, J. Singlet Fission. *Chem. Rev.* **2010**, *110*, 6891–6936.

(2) Smith, M. B.; Michl, J. Recent Advances in Singlet Fission. *Annu. Rev. Phys. Chem.* **2013**, *64*, 361–386.

(3) Shockley, W.; Queisser, H. J. Detailed Balance Limit of Efficiency of P-N Junction Solar Cells. *J. Appl. Phys.* **1961**, *32*, 510–519.

(4) Green, M. A. Third Generation Photovoltaics: Ultra-High Conversion Efficienc at Low Cost. *Prog. Photovolt: Res. Appl.* **2001**, *9*, 123–135.

(5) Nozik, A. J. Quantum Dot Solar Cells. *Physica E* **2002**, *14*, 115–120.

(6) Hanna, M. C.; Nozik, A. J. Solar Conversion Efficiency of Photovoltaic and Photoelectrolysis Cells with Carrier Multiplication Absorbers. *J. Appl. Phys.* **2006**, *100*, 074510.

(7) Berkelbach, T. C.; Hybertsen, M. S.; Reichman, D. R. Microscopic Theory of Singlet Exciton Fission. I. General Formulation. *J. Chem. Phys.* **2013**, *138*, 114102.

(8) Berkelbach, T. C.; Hybertsen, M. S.; Reichman, D. R. Microscopic Theory of Singlet Fission. II. Application to Pentacene Dimers and The Role of Superexchange. *J. Chem. Phys.* **2013**, *138*, 114103.

(9) Scholes, G. D. Correlated Pair States Formed by Singlet Fission and Exciton–Exciton Annihilation. *J. Phys. Chem. A* **2015**, *119*, 12699–12705.

(10) Johnson, J. C.; Nozik, A. J.; Michl, J. The Role of Chromophore Coupling in Singlet Fission. *Acc. Chem. Res.* **2013**, *46*, 1290–1299.

(11) Wang, L.; Olivier, Y.; Prezhdo, O. V.; Beljonne, D. Maximizing Singlet Fission by Intermolecular Packing. *J. Phys. Chem. Lett.* **2014**, *5*, 3345–3353.

(12) Zeng, T.; Hoffmann, R.; Ananth, N. The Low-Lying Electronic States of Pentacene and Their Roles in Singlet Fission. *J. Am. Chem. Soc.* **2014**, *136*, 5755–5764.

(13) Eaton, S. W.; Miller, S. A.; Margulies, E. A.; Shoer, L. E.; Schaller, R. D.; Wasielewski, M. R. Singlet Fission in Thin Films of Tert-Butyl-Substituted Terrylenes. *J. Phys. Chem. A* **2015**, *119*, 4151–4161.

(14) Piland, G. B.; Bardeen, C. J. How Morphology Affects Singlet Fission in Crystalline Tetracene. *J. Phys. Chem. Lett.* **2015**, *6*, 1841–1846.

(15) Pensack, R. D.; Tilley, A. J.; Parkin, S. R.; Lee, T. S.; Payne, M. M.; Gao, D.; Jahnke, A. A.; Oblinsky, D. G.; Li, P.-F.; Anthony, J. E. et al. Exciton Delocalization Drives Rapid Singlet Fission in Nanoparticles of Acene Derivatives. *J. Am. Chem. Soc.* **2015**, *137*, 6790–6803.

(16) Monahan, N.; Zhu, X.-Y. Charge Transfer-Mediated Singlet Fission. *Annu. Rev. Phys. Chem.* **2015**, *66*, 601–618.

(17) Low, J. Z.; Sanders, S. N.; Campos, L. M. Correlating Structure and Function in Organic Electronics: from Single Molecule Transport to Singlet Fission. *Chem. Mater.* **2015**, *27*, 5453–5463.

(18) Müller, A. M.; Avlasevich, Y. S.; Müllen, K.; Bardeen, C. J. Evidence for Exciton Fission and Fusion in a Covalently Linked Tetracene Dimer. *Chem. Phys. Lett.* **2006**, *421*, 518–522.

(19) Johnson, J. C.; Akdag, A.; Zamadar, M.; Chen, X.; Schwerin, A. F.; Paci, I.; Smith, M. B.; Havlas, Z.; Miller, J. R.; Ratner, M. A. et al. Toward Designed Singlet Fission: Solution Photophysics of Two Indirectly Coupled Covalent Dimers of 1,3-Diphenylisobenzofuran. *J. Phys. Chem. B* **2013**, *117*, 4680–4695.

(20) Greyson, E. C.; Stepp, B. R.; Chen, X.; Schwerin, A. F.; Paci, I.; Smith, M. B.; Akdag, A.; Johnson, J. C.; Nozik, A. J.; Michl, J. et al. Singlet Exciton Fission for Solar Cell Applications: Energy Aspects of Interchromophore Coupling. *J. Phys. Chem. B* **2010**, *114*, 14223–14232.

(21) Greyson, E. C.; Vura-Weis, J.; Michl, J.; Ratner, M. A. Maximizing Singlet Fission in Organic Dimers: Theoretical Investigation of Triplet Yield in the Regime of Localized Excitation and Fast Coherent Electron Transfer. *J. Phys. Chem. B* **2010**, *114*, 14168–14177.

(22) Vallett, P. J.; Snyder, J. L.; Damrauer, N. H. Tunable Electronic Coupling and Driving Force in Structurally Well-Defined Tetracene Dimers for Molecular Singlet Fission: A Computational Exploration Using Density Functional Theory. *J. Phys. Chem. A* **2013**, *117*, 10824–10838.

(23) Busby, E.; Xia, J.; Wu, Q.; Low, J. Z.; Song, R.; Miller, J. R.; Zhu, X.-Y.; Campos, L. M.; Sfeir, M. Y. A Design Strategy for Intramolecular Singlet Fission Mediated by Charge-Transfer States in Donor–Acceptor Organic Materials. *Nature Mater.* **2015**, *14*, 426–433.

(24) Trinh, M. T.; Zhong, Y.; Shen, Q.; Schiros, T.; Jockusch, S.; Sfeir, M. Y.; Steigerwald, M.; Nuckolls, C.; Zhu, X.-Y. Intra- to Intermolecular Singlet Fission. *J. Phys. Chem. C* **2015**, *119*, 1312–1319.

(25) Zirzlmeier, J.; Lehnherr, D.; Coto, P. B.; Chernick, E. T.; Casillas, R.; Basel, B. S.; Thoss, M.; Tykwinski, R. R.; Guldi, D. M. Singlet Fission in Pentacene Dimers. *Proc. Natl. Acad. Sci. USA* **2015**, *112*, 5325–5330.

(26) Sanders, S. N.; Kumarasamy, E.; Pun, A. B.; Trinh, M. T.; Choi, B.; Xia, J.; Taffet, E. J.; Low, J. Z.; Miller, J. R.; Roy, X. et al. Quantitative Intramolecular Singlet Fission in Bipentacene. *J. Am. Chem. Soc.* **2015**, *137*, 8965–8972.

(27) Lukman, S.; Musser, A. J.; Chen, K.; Athanasopoulos, S.; Yong, C. K.; Zeng, Z.; Ye, Q.; Chi, C.; Hodgkiss, J. M.; Wu, J. et al. Tuneable Singlet Exciton Fission and Triplet-Triplet Annihilation in an Orthogonal Pentacene Dimer. *Adv. Funct. Mater.* **2015**, *25*, 5452–5461.

(28) Korovina, N. V.; Das, S.; Nett, Z.; Feng, X.; Joy, J.; Haiges, R.; Krylov, A. I.; Bradforth, S. E.; Thompson, M. E. Singlet Fission in a Covalently Linked Cofacial Alkynyltetracene Dimer. *J. Am. Chem. Soc.* **2016**, *138*, 617–627.

(29) Akdag, A.; Havlas, Z.; Michl, J. Search for a Small Chromophore with Efficient Singlet Fission: Biradicaloid Heterocycles. *J. Am. Chem. Soc.* **2012**, *134*, 14624–14631.

(30) Wen, J.; Havlas, Z.; Michl, J. Captodatively Stabilized Biradicaloids as Chromophores for Singlet Fission. *J. Am. Chem. Soc.* **2015**, *137*, 165–172.

(31) Zeng, T.; Ananth, N.; Hoffmann, R. Seeking Small Molecules for Singlet Fission: a Heteroatom Substitution Strategy. *J. Am. Chem. Soc.* **2014**, *136*, 12638–12647.

(32) Bhattacharyya, K.; Pratik, S. M.; Datta, A. Small Organic Molecules for Efficient Singlet Fission: Role of Silicon Substitution. *J. Phys. Chem. C* **2015**, *119*, 25696–25702.

(33) Abbey, E. R.; Zakharov, L. N.; Liu, S.-Y. Electrophilic Aromatic Substitution of a BN Indole. *J. Am. Chem. Soc.* **2010**, *132*, 16340–16342.

(34) Campbell, P. G.; Marwitz, A. J. V.; Liu, S.-Y. Recent Advances in Azaborine Chemistry. *Angew. Chem. Int. Ed.* **2012**, *51*, 6074–6092.

(35) Braunschweig, H.; Geetharani, K.; Jimenez-Halla, J. O. C.; Schäfer, M. Direct Synthetic Route to Functionalized 1,2-Azaborines. *Angew. Chem. Int. Ed.* **2014**, *126*, 3568–3572.

(36) Baggett, A. W.; Guo, F.; Li, B.; Liu, S.-Y.; Jäkle, F. Regioregular Synthesis of Azaborine Oligomers and a Polymer with a syn-Conformation Stabilized by N-H...π Interactions. *Angew. Chem. Int. Ed.* **2015**, *54*, 11191–11195.

(37) Abbey, E. R.; Lamm, A. N.; Baggett, A. W.; Zakharov, L. N.; Liu, S.-Y. Protecting Group-Free Synthesis of 1,2-Azaborines: a Simple Approach to the Construction of BN-Benzenoids. *J. Am. Chem. Soc.* **2013**, *135*, 12908–12913.

(38) Wang, X.-Y.; Zhuang, F.-D.; Wang, X.-C.; Cao, X.-Y.; Wang, J.-Y.; Pei, J. Synthesis, Structure and Properties of C3-Symmetric Heterosuperbenzene with Three BN Units. *Chem. Commun.* **2015**, *51*, 4368–4371.

(39) Koch, M.; Perumal, K.; Blacque, O.; Garg, J. A.; Saiganesh, R.; Kabilan, S.; Balasubramanian, K. K.; Venkatesan, K. Metal-Free Triplet Phosphors with High Emission Efficiency and High Tunability. *Angew. Chem. Int. Ed.* **2014**, *53*, 1–6.

(40) Zhao, Y.; Truhlar, D. G. The M06 Suite of Density Functionals for Main Group Thermochemistry, Thermochemical Kinetics, Noncovalent Interactions, Excited States, and Transition Elements: Two New Functionals and Systematic Testing of Four M06-Class Functionals and 12 Other Functionals. *Theoret. Chem. Acc.* **2008**, *120*, 215–241.

(41) Nakano, H.; Uchiyama, R.; Hirao, K. Quasi-Degenerate Perturbation Theory with General Multiconfiguration Self-Consistent Field Reference Functions. *J. Comput. Chem.* **2002**, *23*, 1166–1175.

(42) Miyajima, M.; Watanabe, Y.; Nakano, H. Relativistic Quasidegenerate Perturbation Theory with Four-Component General Multiconfiguration Reference Functions. *J. Chem. Phys.* **2006**, *124*, 044101.

(43) Ebisuzaki, R.; Watanabe, Y.; Nakano, H. Efficient Implementation of Relativistic and Non-Relativistic Quasidegenerate Perturbation Theory with General Multiconfigurational Reference Functions. *Chem. Phys. Lett.* **2007**, *442*, 164–169.

(44) Li, S. L.; Truhlar, D. G.; Schmidt, M. W.; Gordon, M. S. Model Space Diabatization for Quantum Photochemistry. *J. Chem. Phys.* **2015**, *142*, 064106.

(45) Dunning, T. H. Gaussian Basis Sets for Use in Correlated Molecular Calculations. I. The Atoms Boron Through Neon and Hydrogen. *J. Chem. Phys.* **1989**, *90*, 1007–1023.

(46) Schmidt, M. W.; Baldridge, K. K.; Boatz, J. A.; Elbert, S. T.; Gordon, M. S.; Jensen, J. H.; Koseki, S.; Matsunaga, N.; Nguyen, K. A.; Su, S. et al. General Atomic and Molecular Electronic Structure System. *J. Comput. Chem.* **1993**, *14*, 1347–1363.

(47) Gordon, M. S.; Schmidt, M. W. In *Theory and Applications of Computational Chemistry: The First Forty Years*; Dykstra, C. E., Frenking, G., Kim, K. S., Scuseria, G. E., Eds.; Elsevier: Amsterdam, 2005.

(48) Meyer, H. D.; Manthe, U.; Cederbaum, L. S. The Multi-Configurational Time-Dependent Hartree Approach. *Chem. Phys. Lett.* **1990**, *165*, 73–78.

(49) Beck, M. H.; Jäckle, A.; Worth, G. A.; Meyer, H.-D. The Multiconfiguration Time-Dependent Hartree Method: A Highly Efficient Algorithm for Propagating Wavepackets. *Phys. Rep.* **2000**, *324*, 1–105.

(50) Pasto, D. J. Radical Stabilization Energies of Disubstituted Methyl Radicals. A Detailed Theoretical Analysis of the Captodative Effect. *J. Am. Chem. Soc.* **1988**, *110*, 8164–8175.

(51) Viehe, H. G.; Janousek, Z.; Merenyi, R.; Stella, L. The Captodative Effect. *Acc. Chem. Res.* **1985**, *18*, 148–154.

(52) Alguire, E. C.; Subotnik, J. E.; Damrauer, N. H. Exploring Non-Condon Effects in a Covalent Tetracene Dimer: How Important Are Vibrations in Determining the Electronic Couping for Singlet Fission? *J. Phys. Chem. A* **2015**, *119*, 299–311.

(53) Damrauer, N. H.; Snyder, J. L. Symmetry-Directed Control of Electronic Coupling for Singlet Fission in Covalent Bis-Acene Dimers. *J. Phys. Chem. Lett.* **2015**, *6*, 4456–4462.

(54) Solomons, T. W. G. *Organic Chemistry*, 2nd ed.; John Wiley and Sons, Inc.: New York, 1980.

(55) Tamura, H.; Huix-Rotllant, M.; Burghardt, I.; Olivier, Y.; Beljonne, D. First-Principles Quantum Dynamics of Singlet Fission: Coherent Versus Thermally Activated Mechanisms Governed by Molecular π Stacking. *Phys. Rev. Lett.* **2015**, *115*, 107401.

(56) Varnavski, O.; Abeyasinghe, N.; Aragó, J.; Serrano-Pérez, J. J.; Ortí, E.; López Navarrete, J. T.; Takimiya, K.; Casanova, D.; Casado, J.; Goodson, T. High Yield Ultrafast Intramolecular Singlet Exciton Fission in a Quinoidal Bithiiophene. *J. Phys. Chem. Lett.* **2015**, *6*, 1375–1384.

(57) Chien, A. D.; Molina, A. R.; Abeyasinghe, N.; Varnavski, O. P.; Goodson, T.; Zimmerman, P. M. Structure and Dynamics fo the ^{1}(TT) State in a Quinoidal Bithiophene: Characterizing a Promising Intramolecular Singlet Fission Candidate. *J. Phys. Chem. C* **2015**, *119*, 28258–28268.

(58) Würfel, P. *Physics of Solar Cells: From Basic Principles to Advanced Concepts*; WILEY-VCH Verlag: Weinheim, 2009.